J Therm Anal Calorim (2016) 123:1225–1237
DOI 10.1007/s10973-015-4929-x

Bio-polyamides based on renewable raw materials

Glass transition and crystallinity studies

Joanna Pagacz[1,2] · Konstantinos N. Raftopoulos[1,3] · Agnieszka Leszczyńska[1] · Krzysztof Pielichowski[1]

Received: 3 March 2015 / Accepted: 14 July 2015 / Published online: 5 September 2015

Abstract Structural characterization of a series of novel bio-polyamides based on renewable raw materials—PA 4.10, PA 6.10, PA 10.10, and PA 10.12—was performed by Fourier transform infrared spectroscopy (FTIR) and wide-angle X-ray diffraction (WAXD). Infrared spectra and the WAXD patterns indicate the coexistence of different crystalline forms, α- and γ-triclinic and β-pseudohexagonal. Thermal properties in the glass transition (T_g) and melting region were then investigated using temperature-modulated DSC (TOPEM® DSC). The melting point (T_m) was found to increase with increasing amide/methylene ratio in the polymer backbone, which is consistent with the increase in linear density of hydrogen bonds. Studies on the molecular dynamics by dynamic mechanical analysis show three distinct regions associated with the γ- and the β-relaxation and the dynamic glass transition. TOPEM® DSC data reveal that at low frequency/long timescales, the materials with significantly different amide/methylene ratios have similar segmental dynamics.

Keywords Biopolymers · Glass transition · Molecular dynamics · Differential scanning calorimetry · WAXS · Polymorphism

✉ Joanna Pagacz
jpagacz@chemia.pk.edu.pl

[1] Department of Chemistry and Technology of Polymers, Cracow University of Technology, ul. Warszawska 24, 31-155 Kraków, Poland

[2] Present Address: Wroclaw Research Centre EIT+, ul. Stabłowicka 147, 54-066 Wrocław, Poland

[3] Present Address: Physik-Department, Fachgebiet Physik weicher Materie, Technische Universität München, James-Franck-Str. 1, 85748 Garching, Germany

Introduction

Biopolymers produced from renewable raw materials provide an environmentally friendly alternative to conventional petroleum-based polymers and exhibit new interesting properties, such as low water uptake, high mechanical resistance, high melting point, and crystallization rate [1–4]. Vegetable oils derived from inedible or toxic plants are good alternative chemical feedstock due to their reactivity (numerous active chemical sites) and biocompatibility. They are vastly used for polyurethanes and epoxies; however, durable biothermoplastics, such as bio-polyamides (bio-PAs), based on renewable sources have high growth potential as they show promising mechanical and thermal properties [5–7].

Bio-polyamides are synthesized from two or more monomers or comonomers, which belong to amino acid, cyclic amide (lactam), dicarboxylic acid, and diamine families. Fatty acids present in vegetable oils can be converted by simple reactions into suitable bifunctional monomers for the production of polyamides by a simple polycondensation process. Among most known biomonomers are 11-aminoundecanoic acid and sebacic acid produced by conversion of ricinoleic acid derived from castor oil—Scheme 1.

Typically, raw castor oil is hydrolyzed to give ricinoleic acid, which is then converted to sebacic acid in a reaction with potassium or sodium hydroxide at high temperature [8]. The 1,12-dodecanedioic is most often prepared from petrochemical butadiene, but potentially it can be obtained by an ω-oxidation process of lauric acid catalyzed by yeast strain [9]. Undecane-1,11-dicarboxylic acid and 11-aminoundecanoic acid were reported as potential monomers, too [10]. The diamines for the production of bio-polyamides, e.g., 1,5-diaminopentane (cadaverine),

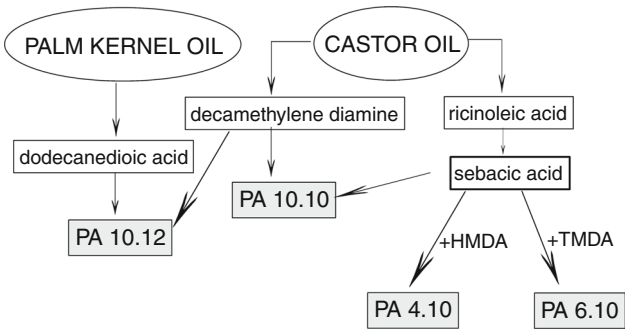

Scheme 1 Schematic route of bio-polyamides production from natural oils

pentamethylenediamine, or tetramethylenediamine, are naturally occurring substances or they can be produced by microbial biosynthesis (e.g., by decarboxylation of amino acids (lysine, ornithine) and polymerization with substances from microbial fermentation (such as succinate) [11–13].

The other way to produce polyamides (PAs) is based on bifunctional monomers; for example, Yamano et al. [14] reported on the preparation of branched polyamide 4 from γ-aminobutyric acid originated from biomass fermentation. The final product was, unlike other polyamides, biodegradable by bacteria isolated from activated sludge. Other bifunctional monomers can be synthesized by complementary hydrobromination of fatty acid methyl esters and further modification [15]. The polyamides with different chain lengths between amide groups (ratio of methylene and amide groups) show different hydrogen bond densities and thus different water absorption. In general, the longer carbon chain results in higher impact strength, higher solvent resistance, and lower water absorption [16, 17]. These characteristics bring possibilities to design novel biobased materials with specially tailored properties.

The degree of crystallinity of polymers, including bio-polyamides, determines their physical and mechanical properties. For semicrystalline materials, a two-phase model of the structure was proposed with a crystalline and an amorphous part, but also a third phase can exist. This phase, the so-called rigid amorphous fraction (RAF), is located at the interfaces between the crystalline and amorphous regions, and is characterized by intermediate properties between two main phases and reduced mobility [18].

Hydrogen bonding plays a significant role in the structure of polyamides, especially in the $2N\ 2(N+1)$ polyamides, i.e., polyamides with equal amounts of methylene groups in the diamine and diacid segment. There are two types of hydrogen bonds that may occur in polyamides—the amide–amide bond and the amide–ester hydrogen bond. Crystals of polyamides were found to be chain-folded and arranged in sheets held together by hydrogen bonds [18]. There are two possible hydrogen-bonded schemes for chain-folded sheets of PAs—the alternating and the progressive one, and they can stack with progressive shearing, yielding the so-called α-phase or with alternating shearing, which is known as the β-phase. In polyamides $2N\ 2(N+1)$, both types of sheet stacking were found, which gives four possible crystal structures [19]. The XRD pattern for these polyamides shows characteristic diffraction peaks related to the interchain and intersheet distance.

Moreover, polymorphism and solid transitions can be observed in polyamides. The former effect is related to the formation of different crystal structures, i.e., the planar α- and the pleated γ-structures, while the latter is an effect of crystal phase transformation prior to melting [20].

The purpose of this work was to study the crystallinity and molecular dynamics of four novel biobased polyamides with variable ratio of methylene and amide groups in the polymer backbone. A novel thermal technique of stochastic modulated-temperature differential scanning calorimetry (DSC TOPEM®) is employed for the study of both phenomena, in comparison and complementarity with well-established techniques of wide-angle X-ray diffraction (WAXD) and dynamic mechanical analysis (DMA). In addition, Fourier transform infrared spectroscopy (FTIR) was used as a complementary method for the study of crystalline and amorphous fraction in polyamides.

Experimental

Materials

The specimens in this study are partly or fully bioresourced polyamides, produced by DSM (PA 4.10, EcoPaXX® Q170MS) and Evonik (*Vestamid* Terra® PA 6.10, PA 10.10, PA 10.12) by polycondensation of adequate diamine and diacid (Scheme 1), with the specifications presented in the Table 1 [16, 21].

The biobased carbon content (BCC) was determined by the producer according to the standard ASTM 6866 and is well above 50 mass% [22]. The PA 10.12 differs in the BCC values, because one of the monomers used for its synthesis, 1,12-dodecanedioc acid, can be sourced both by petroleum production route and via bioproduction from palm kernel oil.

Methods

Processing

For the FTIR, DMA, and WAXD studies, injection-molded samples were used. The pellets of bio-polyamides after

Table 1 Characteristics of bio-polyamides

Bio-PA	Structure	$CONH/CH_2$	$VN/cm^3\ g^{-1}$	BCC/%
PA 4.10	$[–NH(CH_2)_4NHCO(CH_2)_8CO–]$	0.17	170	70
PA 6.10	$[–NH(CH_2)_6NHCO(CH_2)_8CO–]$	0.14	220	63
PA 10.10	$[–NH(CH_2)_{10}NHCO(CH_2)_8CO–]$	0.11	220	100
PA 10.12	$[–NH(CH_2)_{10}NHCO(CH_2)_{10}CO–]$	0.10	220	45–100

VN Viscosity number (ISO 307), *BCC* biobased carbon content (ASTM 6866)

drying (70 °C, 8 h) were processed on an injection molding machine ZAMAK WT 12 at temperature 30 °C above their respective melting points. The mold temperature was kept at 90 °C below the respective crystallization temperature.

Structural characterization

Fourier transform infrared spectroscopy (FTIR) Fourier transform infrared (FTIR) spectra were recorded with a PerkinElmer Spectrum 65 spectrophotometer in ATR mode with C/ZnSe crystal; eight scans with resolution 4 cm^{-1} in the wave number range of 600–4000 cm^{-1} were performed.

Wide-angle X-ray diffraction (WAXD) A Bruker D2Phaser diffractometer with CuKα-radiation ($\lambda = 0.154$ nm) was used to study the crystalline structure of the bio-polyamides. The X-ray diffraction measurements were taken in the reflection mode at room temperature on 1-mm-thick samples (solid bars) produced by injection molding. Bragg's equation, $d = n\lambda/2\sin\theta$, was applied to calculate the interlayer spacing (d_{001}) of the samples by using 2θ-values from the WAXD patterns. Deconvolution of the peaks observed in WAXD analysis was performed with the software Grafity version 0.4.5. The analysis yielded for each reflection peak its position in the 2θ domain, its area, and its full width at half maximum (FWHM).

Thermomechanical characterization

Modulated-temperature DSC (TOPEM®) The DSC with stochastic temperature modulation, provided by Mettler Toledo and branded as TOPEM®, analyzes the dynamic behavior of materials during one single measurement with multifrequency modulation [23]. Step-like temperature perturbations with fixed amplitude and random duration are superimposed to the conventional linear heating, and the heat flow response is recorded. Upon a Fourier transformation, it is possible to calculate the quasi-static heat capacity, $c_{p,0}$, and the frequency-dependent complex heat capacity, c_p^* (ω), at different frequencies and, thus, provide information on the dynamic response of the thermal events. In a more conventional approach of modulated DSC, the stochastic heat flow response may be deconvoluted to its reversing and the non-reversing components, which are related to the thermodynamic and kinetic phenomena, respectively. The method needs to run at sufficiently low heating rate (0.01–2 °C min^{-1}) and small values of temperature perturbation δT_0 (1 mK–0.5 K).

In this work, the melting and the glass transition regions in bio-polyamides were studied in two separate stochastic modulated runs, on fresh as-received samples, each upon a preparatory protocol to remove thermal history and provide good contact with the crucible. Thus, the material was heated up to 280 °C, maintained for 3 min, and then cooled to −10 °C, in a conventional run at a rate of 20 °C min^{-1}. The stochastic modulation runs were performed between −10 and 90 °C for the study of the glass transition region and in varying temperature ranges between 200 and 290 °C, based on preliminary measurements on each sample, for the study of crystallinity. The underlying heating rate was in both cases 0.5 °C min^{-1}, the amplitude of thermal pulses was set at 1 K, and each pulse had a random duration in the range of 15–30 s (switching time range). All measurements were taken in argon. Typical sample mass was about 20 mg, and 20-µl aluminum crucibles were used.

DMA analysis Dynamic mechanical analysis (DMA 242C Netzsch) was carried out on the bars obtained by the injection molding process (area 10 × 26 mm^2, thickness 1 mm) in three-point bending mode (20-mm sample holder) under maximal dynamic force of 6 N, constant part of static force of 0.3 N, and static force 10 % higher than dynamic. The maximal amplitude was set to 50 µm. A temperature scan from −160 to 150 °C was performed at 2 °C min^{-1} and with perturbation frequencies of 1, 2.5, 5, and 10 Hz. Liquid nitrogen was used as cooling medium and dry air as purge. The viscoelastic parameters of storage modulus (E'), loss modulus (E''), and mechanical loss tangent ($\tan\delta$) were recorded as a function of temperature.

Results and discussion

Structural characterization (FTIR)

Figure 1 shows the FTIR spectra of the bio-polyamides. The bands registered for bio-PAs with their respective assignments are summarized in Table 2.

The infrared spectra show characteristic bands for aliphatic polyamides, corresponding to methylene (C–H stretching 2920/2851 cm^{-1}), amide I (C–O stretch 1637 cm^{-1}), amide II (in-plane N–H deformation with CO and CN stretches, ca. 1535 cm^{-1}), and ester group vibrations (1741 cm^{-1}), respectively. The N–H stretching mode appears as a single band at 3300 cm^{-1}, which indicates strong hydrogen bonding, and it is rather broad (Fig. 1), which may suggest that more types of hydrogen bonds with different bond lengths were formed [24]. Moreover, the shape (no shoulders) of the amide I (1637 cm^{-1}) and II bands suggests also that some of the carbonyl groups are hydrogen bonded [25]. This is in agreement with the literature data, indicating that in polyamides two types of hydrogen bonds can be observed, amide–amide and ester–amide, depending on the position of the ester and the amide group along the polymer chain [26].

The bands in the region of 1200–900 cm^{-1} are related to the different crystalline structures in the polyamides. The α-structure should give the absorbance at 1200 and 930 cm^{-1}, and the γ-crystalline phase at 973 cm^{-1} [27]. On the spectra shown in Fig. 1, the bands around 1190 and 942–948 cm^{-1} (C–CO stretching "crystalline" band) confirm the predominant existence of the α-crystalline structure in all tested polyamides. In general, clear differences can be observed in the region 1148–1200 cm^{-1}.

All polyamides show the "crystalline" band at ca. 1190 cm^{-1}; however, its intensity for PA 6.10 is lower than for the other materials. Interestingly, a new band at 1179 cm^{-1} appears for PA 6.10, which is also related to the crystalline domain, but it was found as non-dependent on the crystallinity [27]. This band was also observed for PA 10.10 and 10.12, but at slightly lower frequency of 1165 cm^{-1}. Galimberti et al. [29] attribute the broad band at 1123 cm^{-1} to the amorphous phase related to the chain defects, and it was observed for all bio-PAs.

Moreover, the weak band at 877 cm^{-1} in the spectrum of polyamide 6.10 can be related both to the amorphous region presence and peroxide C–O–O– vibrations, coming from the partial oxidation during processing.

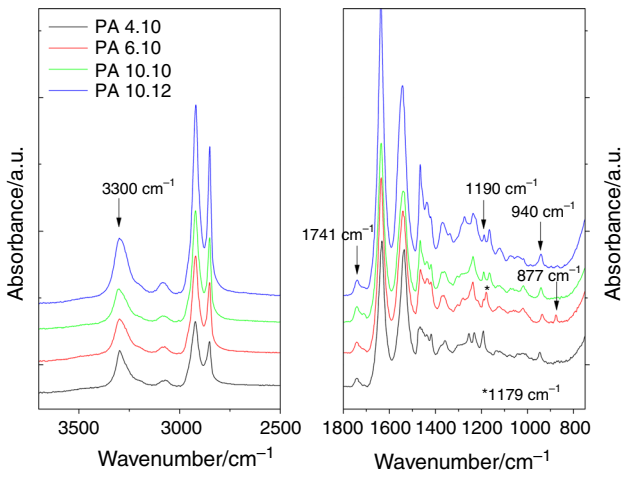

Fig. 1 FTIR spectra of bio-polyamides in different absorbance regions

Crystalline structure (WAXD)

The WAXD patterns of bio-polyamides are presented in Fig. 2.

The characteristic reflection (100) located at about $2\theta = 20°$ and corresponding to the interchain distance in the crystalline structure of the α-crystal form was observed as predominant phase for all samples. The 001 and 002 diffraction peaks at $2\theta \sim 7$ and 10° are related to the length of the chemical repeat unit, but less visible and rather broad.

The relative intensity of the 001 and 002 reflections was found to be governed by the distance between the carbonyl groups in the two alkane segments—if the distance is rather equal, the 001 reflection would be weak because of the destructive interference [34].

A strong reflection located at 23° and assigned to 010/110 crystallographic planes was observed for bio-polyamides, except PA 6.10. Jasińska et al. [24] found similar results for polyamide 4.10 and its copolymers, and they described the peak at $2\theta = 23°$ as characteristic of the γ-crystalline phase. On the contrary, for PA 6.6, Liu and coworkers assign this reflection as one of the distinctive features of the α-phase in polyamides and state that polyamides present usually more stable α-phase rather than γ ones in XRD [20]. In the γ-form phase of the polyamide, hydrogen bonds take position between parallel macrochains, while in α-form the antiparallel arrangement is present, and the latter is more stable because of shorter hydrogen bonds [35].

The scattering patterns for PAs 4.10, 10.10, and 10.12 are comparable, but they present differences in the relative intensity of 100 and 010/110 reflections. This means that the intersheet distance is not affected by the backbone length in the polyamides, while the higher concentration of the amide groups ($CONH/CH_2$ ratio) causes visible changes in the intensity of the 100 peak in comparison with the 010/110 reflection. In PA 4.10, the $CONH/CH_2$ ratio is higher than in PA 10.12, and the intensity of the 001 band increases in relation to 010/110 one. Interestingly, for PA

Table 2 Assignments of the FTIR bands for bio-polyamides

Reference band	Bio-PAs				Band assignment
	4.10	6.10	10.10	10.12	
General					
3300 [28]	3300	3300	3303	3300	N–H stretch hydrogen bonded
3070 [28]	3072	3072	3072	3084	N–H stretch and amide II overtone
2935 [28]	2920	2920	2920	2920	Asymmetric methylene stretch
2860 [28]	2851	2851	2851	2851	Symmetric methylene stretch
1741 [25]	1741	1741	1741	1740	C=O stretch (ester)
1660 [28]	1632	1637	1637	1637	Amide I: C=O stretch
1530 [28]	1535	1535	1535	1537	Amide II: N–H in-plane bending coupled with C–N and C–O stretch
		1541		1542	
1170 [29]	–	1179	1165	1165	CO–NH skeletal, crystalline
1123 [29]	1123 vw	1122	1122	1122 mi	Amorphous
α-structure					
1466 [30]	1466	1466	1466	1466	CH_2 scissoring not adjacent to the amide group
1416 [31]	1419 mi	1419	1419 mi	1420	CH_2 scissoring
1373 [31]	1373 vw	1372	1372	1370	Amide III and CH_2 wagging
1262 [28]	–	1279	–	1273	Amide III
1200 [27]	1192	1192 vw	1191	1188	CH_2 twist-wagging
959 [27]	959 vw	959 vw	959 vw	960 vw	CO–NH in-plane (shoulder)
936 [29]	947	936	942	941	Vibrations of the N-vicinal CH_2 group coupled amide III "crystalline band"
α- and γ-structures					
730 [28]	720 vw	721	721	720	Rocking mode of CH_2
γ-structure					
1439 [32]	1437	1437	1437	1437 mi	CH_2 scissors vibration
1369 [31]	1358	1363	1360	1370	CH_2 twist-wagging
1329 [29]	–	–	–	1336 w	C–H deformation
1236 [33]	1231	1237	1237	1237	CH_2 twist-wagging
1255 [30]	1255	–	–	–	Skeletal C–C stretch
976 [27]	972 vw	972 vw	–	972 vw	CO–NH in-plane

vw Very weak, *w* weak, *m* medium, *mi* more intensive

10.12, the intensities of the 100 and 010/110 reflections are approximately the same, and a weak band can be seen at ca. 21°. This observation may indicate the coexistence of different crystalline forms, α- and γ-triclinic and β-pseudohexagonal structure. The β-mesomorphic structure was identified, e.g., for PA 6 [36]; however, other studies [34, 37] show that only one crystalline phase exists at room temperature in PA 10.12. These discrepancies may come from the different thermal history of the material, resulting in different crystallization conditions.

Meanwhile, the WAXD pattern for PA 6.10 (Fig. 3) differs in the region of 2θ of 21°–25°, and this suggests that only the α-crystalline form is present. However, it is known that the polymorphic structures in polyamides come from different spatial arrangement in the hydrogen bondings; thus, this may be also related to the less perfect crystalline structure of PA 6.10 [35]. On the other hand, FTIR spectra for PA 6.10 show an extra "amorphous" small peak (at 877 cm^{-1}) and a new "crystalline" one (at 1179 cm^{-1}), while the other "crystalline" markers were diminished. This corresponds well with the lack of one missing crystalline diffraction peak in XRD profiles and may indicate that the "crystalline" FTIR band emerging for PA 6.10 at 1179 cm^{-1} (Table 2) corresponds to other α-crystalline structure.

It was reported for PA 6.10 and PA 10.10 that they may exist in two triclinic structures, the α- and the β-structures [38], while for PA 10.12 only one crystalline phase was found [37]. Here, the WAXD results show that bio-PAs, except PA 6.10, may form different crystalline structures

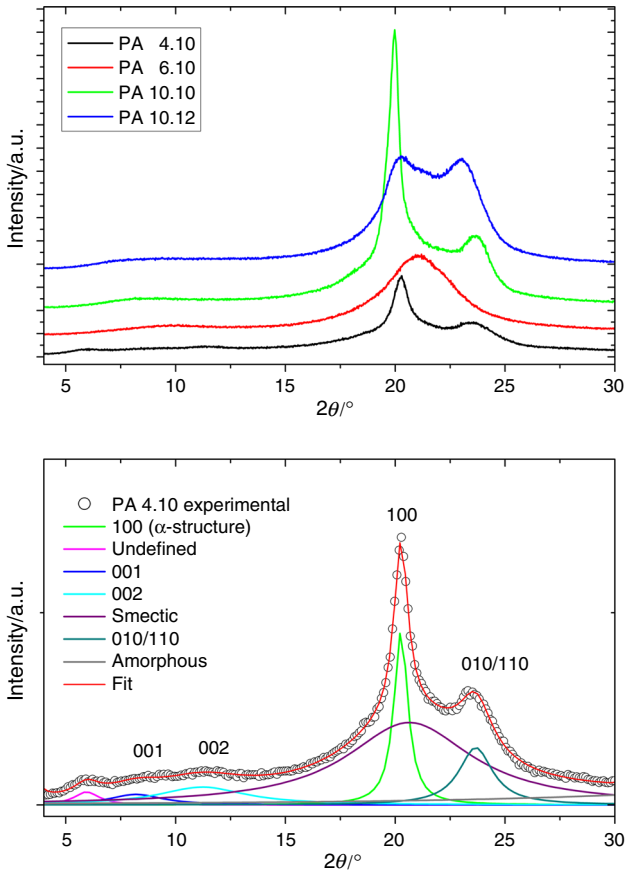

Fig. 2 *Up* WAXD patterns of all bio-polyamides under investigation. *Down* A representative profile fitting result for the PA 4.10

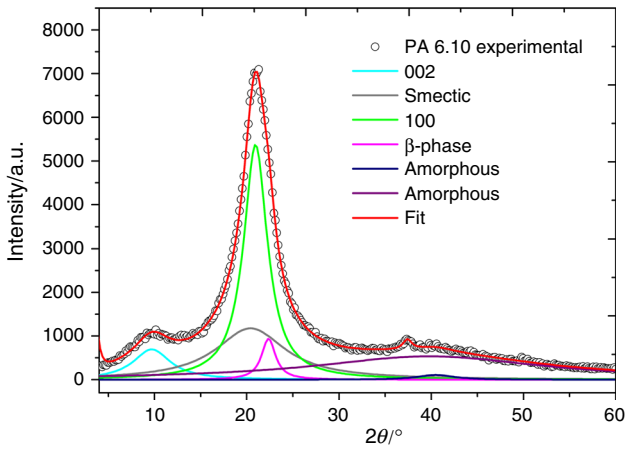

Fig. 3 Fitting profile of WAXD pattern for PA 6.10

depending on the CONH/CH_2 ratio and thus the hydrogen bonding density. In PA 6.10, only one type of crystalline domain was found; however, the method of specimen preparation should be taken into account.

In general, crystallization depends on the energies of the amides and the methylene groups, interchain bonding and chain folding, which are time–temperature characteristics. Quenching of the material will favor the formation of less stable γ-phase, whereas a slow cooling procedure will lead mainly to the formation of more stable crystalline fraction [39]. Considering that the same supercooling state was provided during the processing and the fact that still crystallization may occur at different cooling rates, it can be concluded that the processing of bio-polyamides results in the formation of different crystalline forms.

In order to quantify these observations and calculate the apparent degree of crystallinity ($\chi_{c,WAXD}$), we followed a fitting approach. An adequate fit was achieved with a sum of four Lorentzians to account for crystalline reflections and three Lorentzians more to account for the amorphous halo and the smectic phase. The peak positions of the fitting procedure and the spacings as calculated by Bragg's law are reported in Table 3. Within the experimental inaccuracy, the spacings do not show any significant differences according to the literature for PAs [18, 19, 24, 40]. The amorphous regions are reflected on the smectic peak at 2θ between 18° and 20° and the amorphous halo at ca. 39°. Moreover, the reflections at ~21° can be assigned as γ-phase reflections, formed during quenching from the melt state [35, 41]. The smectic phase found around 20° was also reported for PA 11 using the temperature-dependent X-ray measurements [42, 43]. After deconvolution, a single reflection related to the α-phase was found for PA 6.10 (Fig. 3) at $2\theta = 20.9°$ and another reflection at $2\theta = 22°$, representing the mesomorphic β-form, and this stays in good agreement with the reference data [34, 41].

Concluding, we found that for polyamides used in this study, three crystal phases coexist at room temperature, except PA 6.10, where only the more perfect α-phase and the pseudohexagonal β-phase are present.

Moreover, we calculated the apparent degree of crystallinity, $\chi_{c,WAXD}$, as the ratio of the areas enclosed by the crystalline peaks ($\Sigma A_{crystal}$) to the sum of the areas of the crystalline peaks and the amorphous profile ($\Sigma A_{amorphous}$) [44]:

$$\chi_{c,WAXD} = \left(\frac{\Sigma A_{crystal}}{\Sigma A_{crystal} + \Sigma A_{amorphous}}\right) \times 100 \quad (1)$$

There is no clear dependence of the crystallinity in relation to the amide/methylene ratio; however, the highest crystallinity was found for PA 10.12, in which well-defined structure was observed. The values will be discussed later in relation to the degree of crystallinity evaluated from TOPEM® DSC measurements. However, it was found for polyamides $2N$ ($2N + 1$) that as a length of alkane segments increases, the change in the sheet structure occurs, resulting in change in the chemical nature of lamellar surface [19]. Thus, the crystallinity degree will be affected by the consecutive alkane segments and the CONH/CH_2 ratio.

Table 3 WAXD peak positions and lattice spacings for bio-polyamides under investigation

Bio-PA	Position 2θ/°				Spacings/nm			
	001	002	100	010/110	001	002	100	010/110
PA 4.10	8.2 b	11.2 b	20.1	23.7	1.078	0.789	0.438	0.376
PA 6.10	–	9.7 b	20.9	23.8 vw	–	0.912	0.425	–
PA 10.10	8.3 b	11.9 b	19.9	23.7	1.058	0.742	0.445	0.375
PA 10.12	8.2 b	11.8 b	20.1	23.1	1.072	0.751	0.441	0.384

Other reflections, position 2θ/°

	Undefined	Smectic	β/γ	Amorphous	Undefined	
PA 4.10	5.9	20.6 b	–	38.9	37.7	40.8
PA 6.10	–	20.4 b	22.4	39.8	37.4	40.5 b
PA 10.10	–	19.7 b	21.7 b	38.6	38.6	40.5
PA 10.12	–	18.3 b	21.4	40.3	37.5	40.5

b Broad reflection, *vw* very weak

Melting and crystallization (TOPEM® DSC)

An examination of four bio-polyamides for the melting behavior and the crystallinity was conducted by stochastic modulated DSC (TOPEM®). We used the formalism of the reversing and non-reversing heat flow. The corresponding curves are shown in Fig. 4.

The enthalpy of fusion, ΔH_f, was calculated as the difference in the endothermic melting from the reversing heat flow component (ΔH_{rev}) and the exothermic signal on the non-reversing heat flow profile ($\Delta H_{non\text{-}rev}$): $\Delta H_f = \Delta H_{rev} - \Delta H_{non\text{-}rev}$. The obtained value was further used to calculate the crystallinity degree according to:

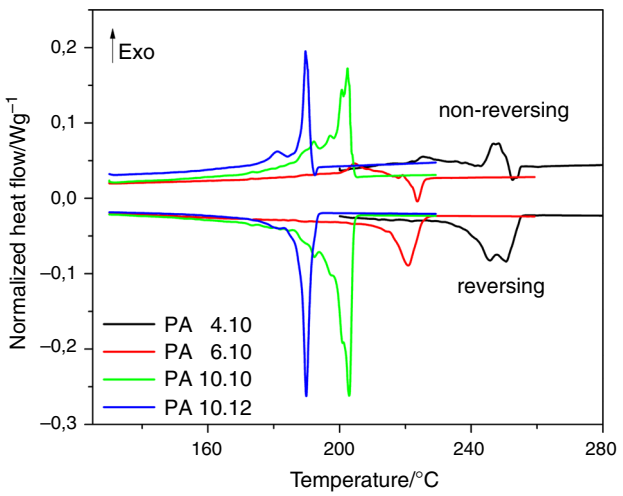

Fig. 4 Reversing and non-reversing TOPEM® signals, recorded during heating for all the bio-polyamides under investigation (at 0.5 °C min^{-1}, amplitude of 1 K, the switching time range of 15–30 s)

$$\chi_{c,DSC} = \frac{\Delta H_f}{\Delta H_f^0} \times 100 \quad (2)$$

where ΔH_f is the experimental enthalpy of fusion (J g^{-1}) and ΔH_f^0 is the reference value of enthalpy of fusion for purely crystalline polyamides. The reference values are 254 and 244 (J g^{-1}) for polyamides 6.10 and 10.10, respectively [38, 45]. To the best of our knowledge, there is no available data for other polyamides. However, considering the chemical similarity of the tested materials, the ΔH_f^0 values for PAs 6.10 and 10.10 were taken as reference values for their closest counterparts, i.e., for PA 4.10 and PA 10.12, respectively. The melting and crystallization points, the associated enthalpies for bio-polyamides, are summarized in Table 4.

The high melting point for PAs was found as the result of the presence of hydrogen bonds which influence the macrochain mobility below T_m and the order of macrochains in the molten state. It was reported that hydrogen bonds may order the crystalline nuclei in the melt and thus influence the subsequent crystallization [39].

The reversing signal contains the melting of outer layers of crystallites. Interestingly, the melting peaks are typically complex with more than one component, corresponding to the two different types of crystal forms as observed by WAXD. In agreement with this interpretation, the reversing heat flow curve of the PA 6.10 shows only one peak corresponding to the α-phase.

The multiple peak of melting in polyamides can be assigned to the fusion of imperfect crystals with lower thermal stability, secondary crystallization upon heating, and remelting of more perfect crystals. Besides, polyamides are known to undergo polymorphic transitions upon heating, and they may form lamellas with different thickness [37, 46, 47].

Table 4 Thermal properties of bio-polyamides by TOPEM® DSC and degree of crystallinity as measured by WAXD

Bio-PA	T_{cp}/ °C	T_m/°C		ΔH_f/J g^{-1}		χ_c/%	
		1	2	Rev	Non-rev	$\chi_{c,DSC}$	$\chi_{c,WAXD}$
PA 4.10	248	246	251	108.63	49.87	23.11	20.54
PA 6.10	205	221	–	113.33	39.47	29.05	36.97
PA 10.10	199	195	–	223.07	155.34	27.76	30.21
PA 10.12	181	190	–	125.72	75.01	20.78	42.87

T_{cp}—Temperature of crystallization during "crystal perfection," T_m—melting point at reversing heat flow curve, ΔH_f—enthalpy of fusion evaluated by integrating the heat flow, $\chi_{c,DSC}$—degree of crystallinity in DSC, $\chi_{c,WAXD}$—degree of crystallinity in WAXD

The melting point (T_m) increases with increasing amide/methylene ratio in the polymer backbone (0.17 for PA 4.10 and 0.1 for PA 10.12). This is consistent with the increasing linear density of hydrogen bonds and was found also for other PAs [19, 48, 49].

The melting starts actually at temperature lower than T_m and can be attributed to slow melting of the material crystallized during the first scan in DSC, which was performed to remove thermal history before temperature-modulated measurements. Upon heating, the less perfect crystals transform to a supercooled state in which recrystallization takes place, what was observed on the non-reversing signal.

The non-reversing component refers processes that are not reversible in the time frame of the modulation, e.g., cold crystallization, melting of the crystallite nuclei, and recrystallization. In the studied polyamides, with the exception of PA 6.10, sharp and strong exotherms occur upon the onset of melting and before the peak melting temperature. These are assigned to the recrystallization or so-called crystal perfection. This is the characteristic event for less perfect crystals, which melt at temperatures below the thermodynamic melting point and then crystallize to another crystal type. This is more notably visible for the PA 4.10, where the recrystallization occurs between the melting of the two types of crystallites.

For the materials with higher amide concentration (PA 4.10 and PA 6.10), a shallow cold crystallization peak occurs in the non-reversing signal, well below the onset of melting. This is related to material that did not have enough time to crystallize during the preceding cooling scan due to slow dynamics. As the temperature increases again, mobility is regained, and the crystallization continues. Apparently, the crystallization dynamics become slower as the amide/methylene ratio increases.

The last phenomenon observed in the non-reversing signal is the final melting of crystal nuclei toward the end of the reversing melting peak. Due to its small intensity, this phenomenon is observed only for the high amide/methylene ratio materials. As the crystalline structure of PA 6.10 is rather simple, no recrystallization occurs, and practically only this nuclei melting peak is present in the DSC curves.

Moreover, when comparing the total heat flow signal with the reversing component, it can be seen that the latter one is much higher than the former, indicating exothermic heat flow of recrystallization and "crystal perfection." Concerning that the melting of semicrystalline polymer is followed by recrystallization and reorganization of remaining crystallites, the total heat flow is the sum of the endothermic heat flow of melting, the exothermic heat flow of recrystallization and reorganization, and the contribution of the heat capacity [50].

The crystallinity-based WAXD measurements correspond well with the one from DSC, except PA 10.12. Although the values are comparable, a clear correlation in these data cannot be given. For semicrystalline polymers, the processing and the thermal history define the thermomechanical features of the material, which in turn determine, e.g., the relaxation, nucleation, and the crystal structure and morphology. Therefore, the processed bio-polyamides differ in their crystal structure from the raw pellets tested in DSC. A more detailed kinetic study of the crystallization dynamics with TOPEM® and isothermal crystallization studies in future work is expected to shed more light in this issue.

Molecular dynamics

Dynamic mechanical analysis (DMA)

Modulus (storage E' and loss E'') and tanδ values of bio-polyamides were recorded as a function of the temperature for different frequencies of mechanical load. Figure 5 shows a comparative plot of E' and tanδ at 5 Hz as a function of temperature.

The DMA curves show three distinct regions, reflected as peaks on the tanδ curves and as downward steps in the E' curves (Fig. 5). Starting from the low-temperature side, and following the tanδ curves, the peak around −150 °C reflects the γ-relaxation, which has been attributed to motions of methylene groups [51]. The composition of the

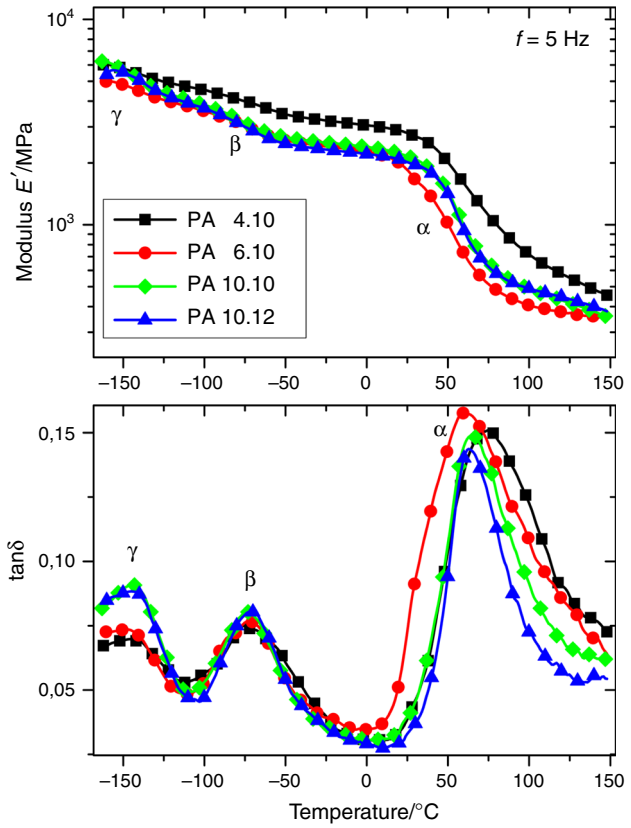

Fig. 5 Storage modulus E' and tanδ curves record with all bio-PAs under investigation, at 5 Hz. For clarity, only every tenth experimental point has been plotted

bio-polyamides does not affect the timescale of this relaxation, confirming its local character. We would like to point out here that a relaxation with very similar timescale characteristics occurs also in polyethers with methylene sequences and their polyurethane copolymers [52], thus supporting the assignment of this relaxation to methylene sequences, in both systems. The strength of the relaxation, as quantified by the height of the peaks (Fig. 5), also supports this assumption.

The next peak around −80 °C is the β-relaxation, typically attributed to non-hydrogen-bonded amide groups [51] and more specifically to water bound on carbonyl groups. Within the experimental error, this relaxation seems unaffected by the length of the methylene sequences between the amide groups, as a result of its strongly localized character. The amide bond is very similar to urethane and urea bonds, having in common the CO–NH sequence. Indeed, a β-relaxation with similar timescale characteristics has been observed in polyurethanes [53], in which it is typically attributed to the same type of molecular motion (i.e., water molecules bound on carbonyl groups) [54]. Interestingly, albeit it is observed by dielectric techniques, a similar relaxation occur also in NH_2 [55]- and OH [52]-terminated polyethers, which denotes that the NH component, too, might have a contribution to this relaxation.

The prominent peak above 50 °C is typically attributed to the dynamic glass transition [56, 57], although some authors dispute it [51]. We will come back to this point, in light of the results by the stochastic modulated DSC results. Nevertheless, we will refer to the peak as the dynamic glass transition (α-relaxation). Its peak temperature T_α is considered as a good measure of the calorimetric glass transition temperature, T_g. In general, the T_g of polyamides drops with increasing mean amide spacing [58, 59]. Here, according to DMA, the PA 4.10 variant seems to have significantly higher T_g than its longer segment counterparts, but otherwise, the other bio-PAs do not follow the trend: With increasing mean amide spacing, the peaks move to slightly higher frequencies as demonstrated in the Arrhenius plot of Fig. 6 and in Table 5.

The dynamics of the α-relaxation is known to follow a Vogel Fulcher Tamman law [60]:

$$f = f_0 \, e^{-\frac{B}{T-T_0}} \tag{3}$$

where f_0, B, and T_0 are parameters to be determined. Nevertheless, the frequency range of the DMA is rather limited for the determination of all three of these parameters, so we may assume a pseudo-Arrhenius behavior:

$$f = f_0 \, e^{-\frac{E_{act}}{kT}} \tag{4}$$

and calculate a pseudo-activation energy upon a linear fitting on the Arrhenius map. The results are again non-monotonous with the amide/methylene ratio: The PA 4.10

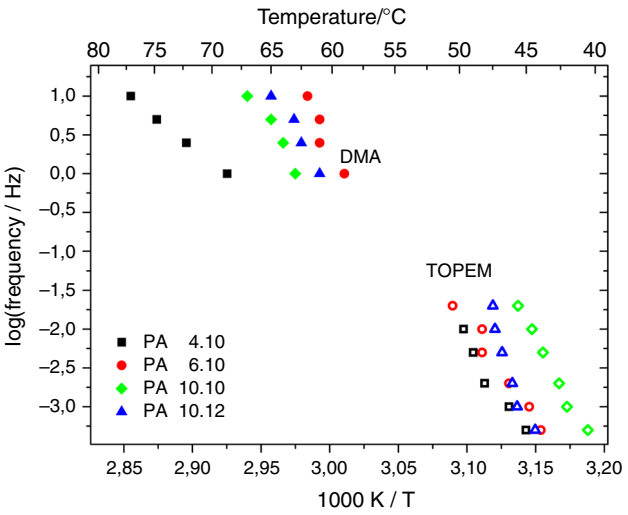

Fig. 6 Arrhenius map in the segmental dynamics region of all materials under investigation. DMA points correspond to the α-peak at tanδ, and stochastic modulated DSC (TOPEM®) points correspond to the Richardson midpoint

Table 5 Glass transition characteristics and α-relaxation pseudo-activation energy in the frequency region of DMA

Bio-PA	TOPEM		DMA	
	T_g/°C	Δc_p/J g^{-1} K^{-1}	T_α/°C	E_{act}/kJ mol^{-1}
PA 4.10	46	0.20	75	270
PA 6.10	45	0.13	61	683
PA 10.10	42	0.14	65	547
PA 10.12	45	0.14	63	532

T_g and Δc_p—heat capacity step at glass transition temperature according to Richardson (1 mHz), T_α—α-relaxation tanδ peak temperature (5 Hz), E_{act}—α-relaxation activation energy in the frequency region studied by DMA, calculated from the Arrhenius plot in Fig. 6

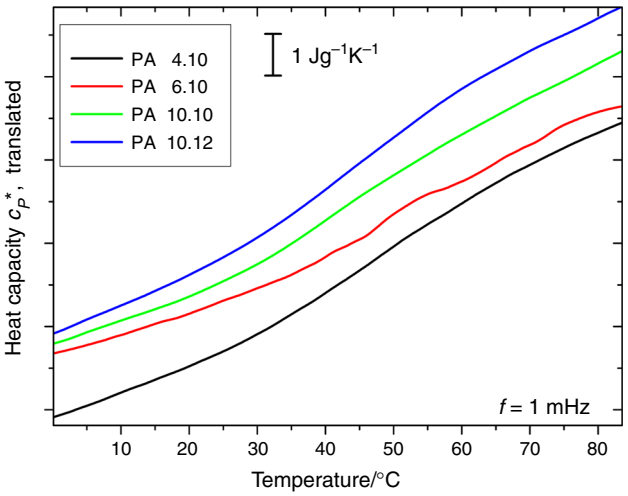

Fig. 7 Stochastic modulated DSC curves in the region of glass transition at 1 mHz. The *curves* have been translated for clarity

has the lowest value, while for the other bio-PAs the E_{act} is a decreasing function of the mean amide spacing, i.e., the average length of the aliphatic components. However, always a higher T_α corresponds to lower activation energy. The discrepancy between the PA 4.10 and other bio-PAs may be related to different technologies for the production of these polymers on industrial scale.

Another interesting point is that the traces of all materials on the Arrhenius map tend to converge toward the low-frequency/low-temperature region. We will come back to this point later upon discussion of the stochastic modulated DSC data in the next section.

The PA 4.10 exhibits higher mechanical modulus, in both the glassy and rubbery regions, than its other homologs, but this may be related, again, to a different manufacturing process. For the PA 6.10, PA 10.10, and PA 10.12, the rubbery modulus is an increasing function of the average distance between amide bonds. However, the glassy modulus remains practically unaffected.

Stochastic modulated DSC (TOPEM®)

In Fig. 7, we plot the magnitude $c_p^*(T)$ of the complex heat capacity as calculated by the Fourier transformation of the response to the stochastic modulated stimulus. The form of this response is similar, from the phenomenological point of view, to heat capacity steps related to glass transition in conventional DSC experiments. However, in stochastic modulated experiments, the temperature location of the step is a function of frequency: The heat capacity is able to follow faster perturbations only at higher temperatures, much similar to what is observed in other types of dynamic experiments such as DMA or dielectric relaxation spectroscopy (DRS).

From the comparative DSC curves (Fig. 7), we cannot draw any straightforward conclusions regarding the dependence of glass transition temperature on the structure of the polyamides; however, we may notice that the heat capacity step Δc_p is an increasing function of the distance between amide groups within the PA 6.10, PA 10.10, and PA 10.12 materials. This may be related to the decreasing degree of crystallinity, as observed with calorimetry, leaving more amorphous material to participate in the segmental dynamics.

As a measure of the glass transition temperature (T_g), we chose the Richardson midpoint [61]. The T_g values obtained by this method for each studied frequency are included in the Arrhenius map in Fig. 6, and as a representative value, we have included the T_g (1 mHz) in Table 5.

Bearing in mind the inaccuracy in determination of the T_g, the traces are located in the same region, with the exception of PA 10.10 which has a significantly lower T_g. Interestingly, the region where the traces are located corresponds well with the one defined by the extrapolation of the DMA traces, bearing in mind the expected concave functional form of the trace of a cooperative relaxation like the dynamic glass transition (α-relaxation). This supports our assignment of the high-temperature peak in the DMA curves to the dynamic glass transition. Experiments with a more broadband technique such as dielectric relaxation spectroscopy are expected to shed more light in the intermediate region between the DMA and TOPEM regions. The reason why the TOPEM trace of the PA 10.10 is located in lower temperatures than expected is yet to be clarified.

In Table 5, we show also the heat capacity step at T_g, Δc_p, as calculated at 1 mHz. The polyamide with the shortest distances between amide groups (PA 4.10) has rather higher Δc_p than its counterparts, which show similar values within the experimental inaccuracy.

Conclusions

Bio-polyamides (bio-PAs) are engineering polymers based on renewable raw materials that link green chemistry approach with good mechanical and thermal properties. In this work, we have performed for the first time the structural characterization of these new polymers, investigated their properties in the glass transition region and studied their molecular dynamics. FTIR analysis revealed that there are characteristic bands for aliphatic polyamides which have been assigned to the functional groups vibrations, such as NH, CO, CONH, and CH_2. Specific interactions by hydrogen bonding were evidenced by the analysis of the N–H stretching mode at 3300 cm^{-1}, which broad profile may suggest that more types of hydrogen bonds with different bond lengths were formed.

In the X-ray analysis, the characteristic reflection (100) located at $2\theta = 20°$ and corresponding to the interchain distance in the crystalline structure of the α-crystal form was observed as predominant phase for all bio-PAs. Interestingly, for PA 10.12, the intensities of the 100 and 010/110 reflections are approximately the same, and the weak band can be seen at ca. 21°—this observation may indicate the coexistence of different crystalline forms, α- and γ-triclinic and β-pseudohexagonal one.

The melting point (T_m) was found to increase with increasing amide/methylene ratio in the polymer backbone, which is consistent with the decreasing linear density of hydrogen bonds. The multiple peak of melting in bio-polyamides can be assigned to the fusion of imperfect crystals with lower thermal stability, secondary crystallization upon heating and remelting of more perfect crystals.

Molecular dynamics investigations by dynamic mechanical analysis (DMA) show three distinct regions associated with γ-relaxation, β-relaxation, and dynamic glass transition. Noteworthy, the composition of the bio-polyamides does not affect the timescale of the γ-relaxation, confirming its local character. Arrhenius map results evidence that the PA 4.10 has the lowest pseudo-activation energy in the 1- to 10-Hz region, while for the other bio-PAs the E_{act} is a decreasing function of the mean amide spacing, i.e., the average length of the aliphatic components. However, always a higher T_α corresponds to lower activation energy. Stochastic modulated DSC results show that at low frequency/long timescales, the materials with significantly different amide/methylene ratios have similar segmental dynamics.

From the methodological point of view, stochastic modulated DSC provides an insight into the segmental dynamics at very low frequencies, which agree very well with those of dynamic mechanical analysis recorded at higher frequencies. However, this point should be followed in future work in more detail, also in comparison and cross-evaluation with more broadband techniques such as dielectric relaxation spectroscopy.

Acknowledgements Authors are grateful to the Polish National Science Center for financial support under Contract No. DEC-2011/01/M/ST8/06834. Authors would also like to thank Dr Daniel Fragiadakis, Naval Research Laboratory, USA, who develops and maintains the software Grafity (distributed free of charge at grafity-labs.com) which we used for our data analysis.

References

1. Kolb N, Winkler M, Syldatk C, Meier MAR. Long-chain polyesters and polyamides from biochemically derived fatty acids. Eur Polym J. 2014;51:159–66.
2. Mohanty AK, Misra M, Drzal LT. Sustainable bio-composites from renewable resources: opportunities and challenges in the green materials world. J Polym Environ. 2002;10:19–26.
3. Swain SK, Patra SK, Kisku SK. Study of thermal, oxygen-barrier, fire-retardant and biodegradable properties of starch bio-nanocomposites. Polym Compos. 2014;35:1238–43.
4. Fan X-D, Deng Y, Waterhouse J, Pfromm P. Synthesis and characterization of polyamide resins from soy-based dimer acids and different amides. J Appl Polym Sci. 1998;68:305–14.
5. Kuciel S, Kuźniar P, Liber-Kneć A. Polyamides from renewable sources as matrices of short fiber reinforced biocomposites. Polimery. 2012;57:627–34.
6. Matadi R, Hablot E, Wanga K, Bahlouli N, Ahzi S, Avérous L. High strain rate behaviour of renewable biocomposites based on dimer fatty acid polyamides and cellulose fibres. Compos Sci Technol. 2011;71:674–82.
7. Hablot E, Matadi R, Ahzi S, Avérous L. Renewable biocomposites of dimer fatty acid-based polyamides with cellulose fibres: thermal, physical and mechanical properties. Compos Sci Technol. 2010;70:504–9.
8. Ranganathan S, Kumar R, Maniktala V. On the mechanism and synthetic applications of the thermal and alkaline degradation of c-18 castor oil. Tetrahedron. 1984;40:1167–78.
9. Lu W, Ness JE, Xie W, Zhang X, Minshull J, Gross RA. Biosynthesis of monomers for plastics from renewable oils. J Am Chem Soc. 2010;132:15451–5.
10. Guillaume L, Jouanneau J, Briffaudd T. Polyamide, composition comprising such a polyamide and their uses. US Patent 20110189419 A1.2011.
11. Hong SH, Kim JS, Lee SY, In YH, Choi SS, Rih JK, Kim CH, Jeomg H, Hur CG, Kim JJ. The genome sequence of the capnophilic rumen bacterium Mannheimia succiniciproducens. Nat Biotechnol. 2004;22:1275–81.
12. Oh IJ, Kim DH, Oh EK, Lee SY, Lee J. Optimization and scale-up of succinic acid production by Mannheimia succiniciproducens LPK7. J Microbiol Biotechnol. 2009;19:167–71.
13. Kind S, Wittmann C. Bio-based production of the platform chemical 1,5-diaminopentane. Appl Microbiol Biotechnol. 2011;91:1287–96.

14. Yamano N, Kawaski N, Nakayama A, Yamamoto N, Aiba S. Novel biodegradable polyamide 4. In: Proceedings of the 2nd Biomass-Asia Workshop, Bangkok, 13–15 Dec 2005.
15. Winkler M, Steinbiß M, Meier MAR. A more sustainable Wohl-Ziegler bromination: versatile derivatization of unsaturated FAMEs and synthesis of renewable polyamides. Eur J Lipid Sci Technol. 2014;116:44–51.
16. Evonik VESTAMID® Terra—Technical information. http://www.vestamid.com/product/vestamid/en/products-services/vestamid-terra/technical-properties/pages/Produktinformationen.aspx. Accessed 29 Nov 2014.
17. Ali MA, Tateyama S, Oka Y, Kaneko D, Okajima MK, Kaneko T. Syntheses of high-performance biopolyamides derived from itaconic acid and their environmental corrosion. Macromolecules. 2013;46:3719–25.
18. Goderis B, Klein PG, Hill SP, Koning CE. A comparative DSC, X-Ray and NMR study on the crystallinity of isomeric aliphatic polyamides. Progr Colloid Polym Sci. 2005;130:40–50.
19. Jones NA, Atkins EDT, Hill MJ, Cooper SJ, Franco L. Polyamides with a choice of structure and crystal surface chemistry. studies of chain-folded Lamellae of Nylons 8 10 and 10 12 and Comparison with the Other $2N$ $2(N + 1)$ Nylons 4 6 and 6 8. Macromolecules. 1997;30:3569–78.
20. Liu X, Wu Q, Berglund LA. Polymorphism in polyamide 66/clay nanocomposites. Polymer. 2002;43:4967–72.
21. DSM EcoPaXX®—Product information. http://www.dsm.com/products/ecopaxx/en_US/product-info.html. Accessed 29 Nov 2014.
22. Standard ASTM D6866 – 12, Standard test methods for determining the biobased content of solid, liquid, and gaseous samples using radiocarbon analysis, http://www.astm.org/Standards/D6866.htm. Accessed 29 Nov 2014.
23. Schawe JEK, Heter T, Hertz C, Alig I, Lellinger D. Stochastic temperature modulation: a new technique in temperature-modulated DSC. Thermochim Acta. 2006;446:147–55.
24. Jasinska L, Villani M, Wu J, van Es D, Klop E, Rastogi S, Koning CE. Novel fully biobased semicrystalline polyamides. Macromolecules. 2011;44:3458–66.
25. Paredes N, Rodríguez-Galá A, Puigallí J. Synthesis and characterization of a family of biodegradable poly (ester amide)s derived from glycine. J Polym Sci, Part A: Polym Chem. 1998;36:1271–82.
26. Kaczmarczyk B, Sek D. Hydrogen bonds in poly(ester amide)s and their model compounds. Polymer. 1995;36(26):5019–25.
27. Vasantham N, Salem DR. FTIR spectroscopic characterization of structural changes in polyamide-6 fibers during annealing and drawing. J Polym Sci, Part B: Polym Phys. 2001;39:536–47.
28. Ishisue T, Okamoto M, Tashiro K. Real-time investigation of crystallization in nylon 6-clay nano-composite probed by infrared spectroscopy. Polymer. 2010;51:5585–91.
29. Galimberti D, Quarti C, Milani A, Brambilla L, Civalleri B, Castiglioni C. IR spectroscopy of crystalline polymers from ab initio calculations: Nylon 6,6. Vib Spectrosc. 2013;66:83–92.
30. Jasinska-Walc L, Dudenko D, Rozanski A, Thiyagarajan S, Sowinski P, van Es D, Shu J, Hansen MR, Koning CE. Structure and molecular dynamics in renewable polyamides from dideoxy–diamino isohexide. Macromolecules. 2012;45:5653–66.
31. Wu Q, Liu X, Berglund LA. FT-IR spectroscopic study of hydrogen bonding in PA6/clay nanocomposites. Polymer. 2002;43:2445–9.
32. Rotter G, Ishida H. FTIR separation of nylon-6 chain conformations: clarification of the mesomorphous and γ-crystalline phases. J Polym Sci B Polym Phys. 1992;30(5):489–95.
33. Nair SS, Ramesh C. Studies on the crystallization behavior of nylon-6 in the presence of layered silicates using variable temperature WAXS and FTIR. Macromolecules. 2005;38(2):454–62.
34. Jones NA, Atkins EDT, Hill MJ, Cooper SJ, Franco L. Chain-folded lamellar crystals of aliphatic polyamides. Investigation of nylons 4 8, 4 10, 4 12, 6 10, 6 12, 6 18 and 8 12. Polymer. 1997;38:2689–99.
35. Ho J-C, Wei K-H. Induced $\gamma \rightarrow \alpha$ crystal transformation in blends of polyamide 6 and liquid crystalline copolyester. Macromolecules. 2000;33:5181–6.
36. Auriemma F, Petraccone V, Parravicini L, Corradini P. Mesomorphic form (β) of nylon 6. Macromolecules. 1997;30:7554–9.
37. Li Y, Zhu X, Tian G, Yan D, Zhou E. Multiple melting endotherms in melt-crystallized nylon 10,12. Polym Int. 2001;50:677–82.
38. Mehta RH. In: Immergut EH, Grulk EA, editors. The polymer handbook. 4th ed. Wiley: New York; 1999; Chapter physical constants of some polymers [Ch. V, p. 126].
39. Murthu NS. Hydrogen bonding, mobility, and structural transitions in aliphatic polyamides. J Polym Sci B Polym Phys. 2006;44:1763–82.
40. Mo ZS, Meng QB, Feng JH, Zhang HF, Chen DL. Crystal structure and thermodynamic parameters of Nylon-1010. Polym Int. 1993;32(1):53–60.
41. Fornes TD, Paul DR. Crystallization behavior of nylon 6 nanocomposites. Polymer. 2003;44:3945–61.
42. Chocinski-Arnault L, Gaudefroy V, Gacougnolle JL, Riviere A. Memory effect and crystalline structure in polyamide 11. J Macromol Sci B Phys. 2002;41:777–85.
43. Ricou P, Pinel E, Juhasz N. Temperature experiments for improved accuracy in the calculation of polyamide-11 crystallinity by X-ray fiffraction. Adv X-Ray Anal. 2005;48:170–5.
44. Alexander LE. X-ray diffraction methods in polymer science. New York: Wiley; 1969. p. 137–97.
45. Feng JH, Mo ZS, Chen DL. Density, equilibrium heat of fusion and equilibrium melting temperature of Nylon 1010. Chin J Polym Sci. 1990;8(1):61–8.
46. Wunderlich B. Macromolecular physics. New York: Academic Press; 1973.
47. Xenopoulos A, Clark ES. In: Nylon plastics handbook. Kohan MI, editor. Munich, Vienna, New York: Hanser Publishers; 1995. Chapter 5.
48. Williams RS, Daniels T. Polyamides. RAPRA Rev Rep 1990;3:Rep.33.
49. Gedde UW. Polymer physics. London: Chapman and Hall; 1995. p. 173.
50. Toda A, Tomita C, Hikosaka M. Temperature modulated DSC of irreversible melting of nylon 6 crystals. J Therm Anal Calorim. 1998;54:623–35.
51. Prevorsek C, Butler RH. Reimschuessel HK. Mechanical relaxations in polyamides. J Polym Sci Part A-2. 1971;9(5):867–86.
52. Raftopoulos KN, Janowski B, Apekis L, Pielichowski K, Pissis P. Molecular mobility and crystallinity in polytetramethylene ether glycol in the bulk and as soft component in polyurethanes. Eur Polym J. 2011;47(11):2120–33.
53. Raftopoulos KN, Jancia M, Aravopoulou D, Hebda E, Pielichowski K, Pissis P. POSS along the hard segments of polyurethane phase separation and molecular dynamics. Macromolecules. 2013;46(18):7378–86.
54. Raftopoulos KN, Pandis C, Apekis L, Pissis P, Janowski B, Pielichowski K, Jaczewska J. Polyurethane–POSS hybrids: molecular dynamics studies. Polymer. 2010;51:709–18.
55. Kosma S, Raftopoulos K, Pissis P, Strachota A, Matějka L, Nedbal J. Molecular mobility of stannoxane modified epoxy resins. J Nanostr Polym Nanocomp. 2007;3(4):144–56.
56. Zhao C, Hu G, Justice R, Schaefer DW, Zhang S, Jang M, Han CC. Synthesis and characterization of multi-walled carbon nanotubes reinforced polyamide 6 via in situ polymerization. Polymer. 2005;46(14):5125–32.

57. Urman K, Otaigbe J. Novel phosphate glass/polyamide 6 hybrids: miscibility, crystallization kinetics, and mechanical properties. J Polym Sci, Part B: Polym Phys. 2006;44(2):441–50.
58. Buchanan DR, Walters JP. Glass-transition temperatures of polyamide textile fibers: part I: the effects of molecular structure, water, fiber structure, and experimental technique. Text Res J. 1977;47:398–406.
59. Saotome K, Komoto H. Polyamides having long methylene chain units. J Polym Sci Part A-1 Polym Chem. 1966;4:1463–473.
60. Donth EJ. The glass transition: relaxation dynamics in liquids and disordered materials. Springer: Berlin, Heidelberg, New York; 2001.
61. Richardson MJ, Savill NG. Derivation of accurate glass transition temperatures by differential scanning calorimetry. Polymer. 1975;16(10):753–7.